Structural and magnetic transitions accompanied by large responses in epitaxial Sr_{0.5}Ba_{0.5}MnO_{3} films

Temuujin Bayaraa, Yurong Yang, Hong Jian Zhao, Jorge Íñiguez, and L. Bellaiche

Phys. Rev. Materials **2**, 084404 — Published 8 August 2018
DOI: 10.1103/PhysRevMaterials.2.084404

Structural and magnetic transitions accompanied by large responses in epitaxial $Sr_{0.5}Ba_{0.5}MnO_3$ films

Temuujin Bayaraa[1], Yurong Yang[1,2], Hong Jian Zhao[3], Jorge Íñiguez[3], L. Bellaiche[1,2]

[1]Physics Department, University of Arkansas, Fayetteville, Arkansas 72701, United States
[2]Institute for Nanoscience and Engineering, University of Arkansas, Fayetteville, Arkansas 72701, United States
[3]Materials Research and Technology Department, Luxembourg Institute of Science and Technology (LIST), 5 avenue des Hauts-Fourneaux, L-4362 Esch/Alzette, Luxembourg.

Abstract

The effect of epitaxial compressive and tensile strains on the physical properties of multiferroic $Sr_{0.5}Ba_{0.5}MnO_3$ films is investigated via the use of *ab-initio* calculations. Striking phenomena are predicted. Examples include (1) the existence of a previously overlooked strain-induced low-symmetry phase bridging the tetragonal (compressively-strained) and orthorhombic (tensile-strained) ferroelectric structures, which exhibits a very large piezoelectric response; (2) a first-order magnetic transition within the tetragonal polar state, which is accompanied by remarkable changes in polarization and out-of-plane lattice constant; (3) the existence of a state that is both ferromagnetic and ferroelectric with a large polarization and axial ratio at large enough compressive strain; and (4) the possibility to induce a structural phase transition between states of different symmetries (e.g., between tetragonal and monoclinic, or between orthorhombic and monoclinic) by applying a magnetic field, which constitutes an original magnetoelectric effect. Experiments are called for to confirm such predictions.

I. INTRODUCTION

The search for multiferroics possessing strong coupling between ferroelectric and magnetic properties is of great interest [1,2], both for technological applications for spintronics and magnonics and for fundamental research in order to understand and optimize such coupling. In particular, promising features of multiferroic materials are a possible control of electric properties by the magnetic field and/or altering magnetic behaviour by applying an electric field. (Sr,Ba)MnO_3 (SBM) perovskites stand out to be an interesting candidate in that respect [3–14], especially because a very large change of polarization has been reported in SBM bulk [7] around the Néel temperature that occurs in the stability range of a tetragonal polar state; that is, when the system becomes antiferromagnetic in addition to remaining polar, which thus makes it multiferroic. $Sr_{1-x}Ba_xMnO_3$ perovskites have also been successfully synthesized [7] and studied [4] as thin films. For instance, it was predicted that not only an orthorhombic ferroelectric state can emerge, but also that a first-order magnetic transition can occur within this orthorhombic phase when varying tensile strain in SBM films. Surprisingly, we are not aware that $Sr_{1-x}Ba_xMnO_3$ films have ever been comprehensively studied for a wider range of strains, that is under tensile but also under small and even large compressive strains, especially via atomistic simulations. It is therefore legitimate to wonder about several issues. For instance, is it possible to play with a strain to create a *low-symmetry* phase bridging higher-symmetry states such as the aforementioned tetragonal and orthorhombic ones? If such hypothetical low-symmetry state exists, will it have giant response properties, in analogy to some morphotropic phase boundary (MPB) compounds [15–22]? One may also ask if the boundaries of such hypothetical strain-induced MPB in SBM may depend on the magnetic ordering, e.g., whether they will vary for different (e.g., G-type antiferromagnetic or ferromagnetic) spin arrangements. If that is the case, one can envision generating a phase transition between two different crystallographic states (e.g., tetragonal and monoclinic) by applying a magnetic field on a SBM film grown on a specific substrate (i.e., for which the epitaxial strain is fixed). Another presently unknown fact about SBM films is whether the application of a large enough compressive strain can render such systems ferromagnetic, thus departing from their antiferromagnetic ground state, and whether such an effect can also have structural implications as regards the polarization and the strain state. In other words, may SBM films allow us to fulfil one strongly desired goal in the field of multiferroics, namely to discover a multiferroic compound that is ferromagnetic, strongly polar and with a large axial ratio, with all these properties being controllable by an external factor (namely, compressive strain here) [23]?

The goal of this article is to positively answer all these open questions by performing and analyzing first-principles calculations. This article is organized as follows. Section II provides computational details. Section III reports our results, and a summary is given in Section IV.

II. COMPUTATIONAL DETAILS

Here, and in analogy to Refs [3–6], we mostly considered a specific chemically-ordered structure of multiferroic $Sr_{0.5}Ba_{0.5}MnO_3$ (SBM), since mimicking chemically-disordered SBM solutions is beyond the current reach of first-principles calculations (because it requires the use of very large supercells). Note that we also chose to study an overall composition of 0.5 because it is known [7] that the perovskite structure cannot be synthesized for large Ba compositions and that Sr1-

$_{x}$Ba$_{x}$MnO$_{3}$ is multiferroic (namely, ferroelectric in addition to be magnetically-ordered) only for Ba compositions larger than 40%. Our chosen structure exhibits a rock-salt ordering between its Ba and Sr atoms, is denoted as "DP" (for double perovskites) and is shown on the left side of Fig. 1. We chose a $\sqrt{2}\,x\,\sqrt{2}\,x\,2$ simulation cell that has 20 atoms to accommodate all four magnetic orderings commonly found in manganites, namely, ferromagnetic (FM), A-type antiferromagnetic (A-AFM), C-type antiferromagnetic (C-AFM) and G-type antiferromagnetic (G-AFM) [24]. We consider epitaxial films being under compressive or tensile strains. For any chosen in-plane lattice parameter, a_{ip}, the in-plane lattice vectors are frozen in our simulations with their length being directly proportional to this a_{ip}. All the other structural degrees of freedom, including the out-of-plane lattice vector and atomic positions, are allowed to relax in order to minimize the total energy until residual forces are smaller than 0.001 eV/Å. Typically, we allow the in-plane lattice parameter to range between 3.78Å and 4.11Å in our simulations. We used the Vienna ab initio simulation package (VASP) [25] to conduct density functional theory (DFT) calculations [26,27]. All simulations are performed using a PBE+U+J functional [28,29] and the projector augmented-wave potentials [30,31]. The Hubbard U value on Mn atoms is chosen to be 2.0 eV, 3.0 eV or 4.5 eV (in order to check the influence of U on physical properties) while the Hund J value is taken to be 1.0 eV, as similar to Ref. [5]. The energy cutoff is selected to be 550 eV, and the k-point mesh is chosen to be 6x6x4. The polarization is calculated by the Berry phase method [32] and space groups are identified using the Isotropy software [33]. Note that we also used the PBEsol functional [41] with Hubbard U corrections (with U=2eV, 3eV, 4.5eV) and Hund J=1.0 eV to compute properties of epitaxial SBM films within the DP structure. Surprisingly, we numerically found that the phase having the lowest possible energy over the whole range of investigated a_{ip} is non-polar in that case, which contradicts the experimental discovery of a polar tetragonal state in SBM bulk [7].

III. EPITAXIAL-STRAIN-INDUCED PHASE TRANSITIONS

a. PHASE DIAGRAM

Let us first select U= 3 eV and J=1 eV (note that section III.d explains such choice). Figure 2(a) displays the total energy as a function of the in-plane lattice constant for the four aforementioned magnetic configurations. It is important to realize that, for any of these magnetic arrangements, (1) smaller in-plane lattice constants (which correspond to compressive strains) favor a tetragonal *I4mm* state; (2) larger a_{ip}'s (i.e., tensile strains) yield an orthorhombic *Imm2* ground state; and (3) intermediate in-plane lattice parameters result in the emergence and stabilization of a monoclinic *Cm* phase. Interestingly, all these three states are polar in nature. A tetragonal polar state has been previously observed in SBM bulks and films [7], but with a *P4mm* symmetry rather than *I4mm*. Such a difference simply reflects the fact that our studied structure is chemically ordered, while typical experimental samples are chemically disordered. Moreover, data consistent with an orthorhombic polar state (namely, atomic displacements being along the pseudo-cubic [110] direction) have been reported in Refs. [4,9] for SBM films under tensile strains. On the other hand, we are not aware of any study reporting any monoclinic state in these materials. As further shown in Fig. 2a, the values of the total energy at the minima of the tetragonal *I4mm* and orthorhombic *Imm2* states are both strongly dependent on the kind of magnetic order (as consistent with Ref. [4] for films under tensile strain), since they significantly increase when going from G-AFM to FM, via C-AFM and A-AFM. Moreover, the in-plane lattice parameters corresponding to these minima also depend strongly on the spin arrangement. For instance, focusing on the minima of the orthorhombic *Imm2* state, a_{ip} is equal to about 3.92Å for the G-AFM configuration, while it gets close to 4.0Å in the FM case. Consequently, some in-plane lattice parameters correspond to different structural states for different magnetic arrangements! For example, the ground state associated with a_{ip} = 3.92Å is *Imm2* for both G-AFM and C-AFM, but it becomes monoclinic *Cm* for A-AFM and FM orders. Such a remarkable behaviour strongly suggests that it is possible to alter the symmetry of the structural phase by applying magnetic fields in some epitaxial SBM thin films grown on appropriate substrates, which constitutes a giant and novel magnetoelectric (ME) effect. As a matter of fact, one can envision going from a G-AFM orthorhombic state into a FM monoclinic state under magnetic fields for a_{ip} values around 3.92Å. Moreover, Fig. 2a also suggests that a G-AFM tetragonal state can transform into a FM monoclinic state, by applying a magnetic field, for a_{ip} around 3.859Å. In fact, based on the computed energy differences, we estimated the required magnetic field to induce such tetragonal-to-monoclinic structural phase transition to be ~120T in the DP structure for a_{ip} = 3.859Å. It is conceivable that such magnetic field can decrease in magnitude (which will make it more physically feasible) when increasing the temperature, since the free energies of AFM and FM states will get closer to each other when heating a magnetic system.

b. MAGNETIC PHASE TRANSITIONS

Another striking feature indicated by Fig. 2a is that strain can induce magnetic transitions. Note that the SBM films adopt a G-AFM ordering for a_{ip} between 3.8038Å and 3.9706Å (while moving from *I4mm* to *Cm* and finally to the *Imm2* polar states). Yet, ferromagnetism is energetically preferred for in-plane lattice constants below 3.8038Å (with the A-AFM order being rather close in energy); further, the films transform into C-AFM for a_{ip} larger than 3.9707Å, and then to ferromagnetism for in-plane lattice constants larger than 4.0877Å. Note that magnetic transitions from G-AFM to C-AFM, and then to ferromagnetism, have also been reported in Ref. [4] for tensile strains (i.e., within an orthorhombic state), but we are not aware that any strain-induced magnetic transition towards ferromagnetism has been previously documented for SBM films under compressive strain (which yields a tetragonal state according to our calculations). In particular, our predictions strongly suggest that growing SBM films on substrates with small lattice constants, such as the commonly used $LaAlO_3$ and $YAlO_3$ that have lattice parameters of the order of 3.7-3.8Å [34,35], should yield SBM films being FM and polar. (Note that, by comparing measurements and calculations for pure $SrMnO_3$, we estimate that the present PBE+U+J computations with U=3eV and J=1eV provide an overestimation of about 0.5% for the lattice constants. Such small overestimation demonstrates the rather high accuracy of our calculations).

c. POLARIZATION AND MONOCLINIC REGION

Let us now concentrate on the different structural and magnetic *ground states*, that are: FM *I4mm* for in-plane lattice constants below 3.8038Å; G-AFM *I4mm* for a_{ip} between 3.8038Å and 3.879Å; G-AFM *Cm* for a_{ip} between 3.879Å and 3.90Å; G-AFM *Imm2* for a_{ip} between 3.90Å and 3.9707Å; C-AFM *Imm2* for a_{ip} between 3.9707Å to 4.0877Å; and FM *Imm2* for a_{ip} larger than 4.0877Å. The total electric polarization of these different ground states is displayed (in their stability regions) in Fig. 2b as a function of the in-plane lattice constant, with the vertical dashed lines representing magnetic phase transition points. Figure 2c reports the corresponding behaviour of the axial ratio, c/a_{ip}. One can clearly see sudden jumps of both polarization components when the films undergo (first-order) magnetic phase transitions, which indicates large magnetoelectric couplings. Additionally, we also find discontinuities in the aspect ratio associated to the spin transformations, suggesting the possibility to have colossal magnetostrictive effects. In particular, at the G-AFM-to-FM transition point for a_{ip} around 3.8038Å, the total electric polarization dramatically jumps from 0.443 C/m^2 to 0.606 C/m^2, while c/a is strongly enhanced from 1.07 to 1.11, within the tetragonal I4mm state (note that we are not aware that such large jumps have ever been observed in any multiferroics). Such magnetic-induced enhancement of the polarization hints (as consistent with Ref. [4]) at the existence of an energetic term of the form $\Delta E = C\, P^2_z\, (\mathbf{m}_1 \cdot \mathbf{m}_2)$ in the tetragonal phase of SBM, where P^2_z is the square of the z-component of the polarization while $\mathbf{m}_1$ is the magnetic moment averaged over every other Mn ion (along any pseudo-cubic <100> direction) and $\mathbf{m}_2$ is the magnetic moment averaged over all the remaining Mn ions. In this term, the C coefficient should be rather strong in magnitude and *negative*, therefore enhancing the polarization of the *I4mm* state when going from antiferromagnetism (for which the dot product $\mathbf{m}_1.\mathbf{m}_2$ is negative) to ferromagnetism (for which the dot product $\mathbf{m}_1.\mathbf{m}_2$ term is positive). Note that such suggested energetic term and strong, negative C coefficient are also fully consistent with the striking observation [7] that the polarization and associated axial ratio both significantly decrease with temperature around the Néel point in SBM bulk, that is, when the system transforms from paramagnetic (for which $\mathbf{m}_1 \cdot \mathbf{m}_2$ is essentially null, since both the averaged $\mathbf{m}_1$ and $\mathbf{m}_2$ vanish) to G-AFM within the ferroelectric tetragonal state of SBM bulk. Figure 2b further indicates that the total electric polarization of the *Imm2* orthorhombic state remarkably increases from 0.299 C/m^2 to 0.334 C/m^2 for a_{ip} around 3.9707Å (as consistent with the different magnitude of atomic displacements found in Ref. [4] between the G-AFM and C-AFM arrangements at this magnetic transition), which hints at another energetic term of the form $\Delta E = D\, (P^2_x + P^2_y)\, (\mathbf{m'}_1.\mathbf{m'}_2)$, in the orthorhombic state, where D is a negative coefficient, P^2_x and P^2_y are the squares of the x- and y-components of the polarization, and $\mathbf{m'}_1$ and $\mathbf{m'}_2$ are magnetic moments of Mn ions that are the first-nearest neighbor of each other along the z-axis. Moreover, the polarization also weakly increases from 0.430 C/m^2 to 0.444 C/m^2 for a_{ip} around 4.0877Å, that is, when the C-AFM-to-FM transition occurs. The axial ratio slightly increases from 0.961 to 0.964 and from 0.921 to 0.922 at these two latter magnetic transitions, respectively. It is worthwhile noting that Fig. 2b demonstrates that the polarization of the FM tetragonal phase (in the compressive regime) is much larger than that of the FM orthorhombic state (in the tensile regime), namely by about 35%. Figure 2b further shows that, as commonly observed in perovskite films (see, e.g., Ref. [20] for $PbTiO_3$ films), (i) the structural region of SBM with the *I4mm* space group has a polar axis along the pseudo-cubic out-of-plane [001] that increases, along with c/a, when decreasing a_{ip}; and (ii) the orthorhombic region of SBM with the *Imm2* space group has a polar axis along the pseudo-cubic [110] direction that is enhanced, while c/a decreases, when the in-plane lattice parameter is increasing [20]. On the other hand, if we concentrate on the newly found, low-symmetry monoclinic region with space group *Cm* (which is a subgroup of both *I4mm* and *Imm2*), a continuous rotation of the polar axis between the pseudo-cubic [001] and [110] directions, as well as a concomitant continuous decrease of the axial ratio from values larger than 1 to values smaller than unity, occur when progressively increasing a_{ip}. In other words, a strain-induced morphotropic-like phase boundary exists in SBM films, which bears resemblance with the compositional, pressure or strain areas bridging two different high-symmetry ground states via a monoclinic state in some other perovskites (e.g., $Pb(Zr_{1-x}Ti_x)O_3$, $PbTiO_3$, $BiFeO_3$, or $(Ba_{1/2}Na_{1/2})TiO_3$-$BaTiO_3$) [15–20]. The present prediction of a bridging monoclinic phase in SBM films is thus of high importance when recalling that such low-symmetry phases have been shown to exhibit large physical responses, such as high piezoelectricity, dielectric and elasto-optic responses [16,20–22]. As consistent with these well-known facts, we further numerically found here that the e_{33} piezoelectric coefficient of the G-AFM Cm phase of SBM is as large as 16 C/m^2 for a_{ip} = 3.899Å, that is, more than four times bigger than the one predicted for the prototype ferroelectric (tetragonal) $PbTiO_3$ system and about twice as large as that of the "giant-piezoelectric" (tetragonal) $0.6Pb(Mg_{1/3}Nb_{2/3})O_3+0.4PbTiO_3$ (PMN-PT) compound (see Ref. [36] and references therein)

Note that our predicted a_{ip} range for the G-AFM *Cm* state is between 3.879Å and 3.90Å which, after rescaling by the expected overestimation of 0.5% mentioned above, become 3.86Å and 3.88Å, respectively. Interestingly, this corrected range of 3.86-3.88Å encompasses the pseudo-cubic lattice constant of $(La,Sr)(Al,Ta)O_3$ (LSAT) which is about 3.867Å [9]. Such fact suggests that the growth of $Sr_{0.5}Ba_{0.5}MnO_3$ (SBM) epitaxial films on LSAT should lead to the observation of our predicted monoclinic state and its accompanying large response, according to our calculations. This possibility is even further realizable in our minds, when recalling that the perovskite phase of $Sr_{1-x}Ba_xMnO_3$ has been recently synthesized for compositions *x* varying between 0.2 and 0.5 on *several* substrates [14].

Let us now pay a particular attention to the monoclinic *Cm* state presently reported in SBM films. Figure 2a tells us that, unlike the tetragonal *I4mm* and orthorhombic *Imm2* states, the monoclinic Cm phase does not adopt a minimum in energy as a function of a_{ip}, but rather displays a local maximum. This maximum is located at about a_{ip} = 3.89Å and 3.94Å for the G-AFM and FM arrangements, respectively, and is indicated by arrows in Fig. 2a. Such local maximum also seems to exist in other epitaxial films (such as $PbTiO_3$, see Fig. 1 of Ref. [20]) for which the structural bridging between the analogous tetragonal and orthorhombic ferroelectric phases also occurs via a monoclinic *Cm* state. It appears, in fact, to be linked with the rotation of the polarization within the *Cm* phase. As a matter of fact, and as shown in Fig. 2b, in the case of the G-AFM arrangement, the out-of-plane component of the polarization is smaller than its plane-component for a_{ip} above 3.90Å (i.e., close to the maximum for the G-AFM monoclinic phase) while the reversed situation holds for smaller a_{ip}. Similarly, in the case of the FM arrangement, the out-of-plane component of the polarization gets smaller than its plane-component when $a_{ip} > 3.93$Å (i.e., now near the maximum of the FM monoclinic phase) while the opposite hierarchy happens when $a_{ip} < 3.93$Å. Furthermore, to check the stability of the newly found monoclinic phase, we also report the computed lowest optical frequency at the Γ-point for the G-type AFM configuration as a function of the in-plane lattice parameter in Figure 3. One can see that the frequency of the lowest optical phonon mode of the tetragonal state becomes negative as the in-plane lattice constant gets larger than 3.87Å and, similarly, the frequency of the lowest optical phonon mode of the orthorhombic state is also negative as the in-plane lattice constant gets smaller than 3.91Å. As a result, the tetragonal and orthorhombic states are dynamically unstable for in-plane lattice constants ranging between 3.87Å and 3.91Å. A new structure (with positive phonon frequency) thus has to emerge within this in-plane lattice constant region, which is precisely our presently discovered monoclinic state.

d. INFLUENCE OF THE RESULTS ON THE U PARAMETER AND CHEMICAL ORDERING

Let us now pay attention to the influence of the U parameter on physical results. For that, Table 1 reports the value of the polarization, in-plane lattice constant and axial ratio of the predicted equilibrium tetragonal state of $Sr_{0.5}Ba_{0.5}MnO_3$ bulk, as mimicked by the DP structure (this tetragonal state is of *I4mm* symmetry), for U=2, 3 and 4.5 eV and J=1.0 eV. Increasing U (i) decreases this polarization; (ii) enhances the in-plane lattice constant; and (iii) reduces this axial ratio. In particular, comparing our predicted polarizations shown in Table 1 with the estimated value of 0.135 C/m^2 *indirectly* extracted from low-temperature measurements in Ref. [7] suggests that using U=4.5eV may provide the best agreement with such measurements. However, Figure 4 shows that high values of the Hubbard parameter for Mn (such as U= 4.5 eV) results in an incorrect result for the SBM films, as mimicked by the DP configuration, namely that the orthorhombic minimum is of lower energy than the tetragonal one – which contrasts with the observed tetragonal symmetry of SBM bulks [7]. In other words, the energy difference between orthorhombic and tetragonal states minima is affected by the choice of Hubbard U. One should in fact choose a small U, such as 2 eV, when desiring to have the tetragonal state being the lowest one and the furthest away in energy from the orthorhombic phase. Compromising between such desire and the conflicting wish to agree with indirect low-temperature measurements for the magnitude of the polarization in tetragonal $Sr_{0.5}Ba_{0.5}MnO_3$ bulk motivated us to select the intermediate U=3 eV in this work. Figure 4 further shows that different choice of Hubbard U affects the in-plane lattice parameters at which the G-type antiferromagnetic (AFM) to ferromagnetic (FM) magnetic phase transition occurs in the compressive regime within the polar tetragonal state. Moreover, and for both the G-type AFM and FM arrangements, as we lower the Hubbard U value, the a_{ip} at which the tetragonal-to-monoclinic transition occurs gets smaller while the a_{ip} of the monoclinic-to-orthorhombic transition gets larger (therefore widening the stability region of the monoclinic phase). Furthermore, to address the stability of different magnetic states, the energy of the equilibrium tetragonal phase of the A-AFM, C-AFM and FM configurations with respect to the G-AFM arrangement is reported in Table 2 for different values of Hubbard U for $Sr_{0.5}Ba_{0.5}MnO_3$ bulk (keeping J=1 eV in all these calculations), as modeled by the DP structure. Increasing U from 2 to 4.5 eV brings the A-AFM, C-AFM and FM states closer in energy to the G-AFM configuration but does not change the energetic hierarchy (that is the G-AFM state is the lowest in energy followed by C-AFM, A-AFM and then FM). Also, the influence of the Hubbard U parameter on the magnetic moment is shown in Tables 1 and Table 2. Overall, for all four magnetic arrangements, increasing the Hubbard U value enhances the magnetic moments on Mn ions.

Note that, in addition to the DP structure, we also studied another chemical ordering for epitaxial $Sr_{0.5}Ba_{0.5}MnO_3$ films. It is denoted as the "DL" (for double layers) structure and has alternating (001) layers made of Ba or Sr atoms. Such structure is depicted on the right side of Fig. 1. We report, in Fig. 5, properties of such structure as a function of the in-plane lattice constant, when using the PBE+U+J functional with U=3 eV and J=1.0 eV.

One can see that the important qualitative results of the DP structure (namely, (i) the existence of a monoclinic phase that bridges two high-symmetry phases; (ii) the occurrence of a polar ferromagnetic tetragonal state at large enough compressive strain; and (iii) large jumps of polarization and axial ratio when crossing magnetic transitions under compressive strain) are also found in the DL structure. Such facts imply that items (i)-(iii) should all be found regardless of chemical ordering, and therefore should also occur for chemically-disordered SBM films. Note that one qualitative difference between the results of the DP and DL structures is that the magnetic ground state prefers a C-AFM rather than a FM ordering in some compressive regions in the DL structure, implying that there is a G-AFM-to-C-AFM transition (and then a C-AFM-to-FM transition) in DL *versus* a (direct) G-AFM-to-FM transition in the DP structure when enhancing the magnitude of the compressive strain. Interestingly, a G-AGM-to-C-AFM transition and a G-AFM-to-FM transition share the common feature that the spin configuration of two Mn neighbors along the in-plane [100] and [010] directions changes from anti-parallel to parallel. Another qualitative difference between the DP and DL structures is the space group of the tetragonal and orthorhombic states, namely I4mm *versus* P4mm and Imm2 *versus* Amm2. Such changes are simply originating from chemical ordering.

IV. SUMMARY

We have studied the influence of epitaxial strain, both in the compressive and tensile regimes, on the properties of $Sr_{0.5}Ba_{0.5}MnO_3$ films. One particularly striking result is the discovery of a strain-induced morphotropic phase boundary in SBM films, which presents a previously overlooked monoclinic phase bridging the known tetragonal and orthorhombic states – with this low-symmetry phase having, e.g., a large piezoelectric response. Such monoclinic state exhibits a local maximum in its energy-*versus*-in-plane lattice constant curve, which is related to the rotation of the electric polarization. Another important finding is the occurrence of a strain-induced transition towards an insulating polar and ferromagnetic (and thus multiferroic) state having a large polarization and large axial ratio in the compressive part of the studied phase diagram. Large jumps of polarization and axial ratio are found when crossing magnetic transition under compressive strain, strongly hinting at the realization of giant magnetoelectric couplings and magnetostriction (note that connections between structural distortions and magnetic properties have also been found in other types of Mn-based materials such as Heusler compounds [37,38]). It is also worthwhile to emphasize that our calculations further suggest a very peculiar magnetoelectric effect, that is, a phase transformation from a (high-symmetry) tetragonal or orthorhombic state to a (low-symmetry) monoclinic state via the application of a magnetic field. Note also that Ref. [39] predicted the existence of a ferroelectric and ferromagnetic tetragonal state at large enough compressive strain, as well as sudden large changes of the polarization and axial ratio when passing through a strain-induced magnetic transition. However, such predictions were for films made of $SrMnO_3$ perovskite and consequently occur for compressive strains that are likely too large to be realistic. Moreover, according to Ref. [39], the $SrMnO_3$ films will not present a ferroelectric monoclinic phase, as for moderate epitaxial deformations this material presents a paraelectric ground state. We thus call for experimental confirmations of all our predictions in SBM epitaxial films, especially since we provide examples of substrates that can be practically used to observe such effects. In particular, it will be interesting to determine if such monoclinic phase can be detected and is more thermodynamically stable than the coexistence of domains with different symmetries [40].

T.B. and L.B. thank the Office of Basic Energy Sciences, under contract ER-46612. Y.Y. acknowledges the ONR Grants N00014-12-1-1034 and N00014-17-1-2818. We also acknowledge funding from the Luxembourg National Research Fund through the inter-mobility (Grant 15/9890527 GREENOX, L.B., H.J.Z and J.I.) and Pearl (Grant P12/4853155 COFERMAT, H.J.Z. and J.I.) programs. We also thank the Arkansas High Performance Computer Center at the University of Arkansas for access to the supercomputers. T.B. acknowledges Fulbright Mongolia Government Scholarship.

References:

[1] W. Eerenstein, N. D. Mathur, and J. F. Scott, Nature **442**, 759 (2006).

[2] R. Ramesh and N. A. Spaldin, Nat. Mater. **6**, 21 (2007).

[3] H. Chen and A. J. Millis, Phys. Rev. B **93**, 205110 (2016).

[4] H. Chen and A. J. Millis, Phys. Rev. B **94**, 165106 (2016).

[5] G. Giovannetti, S. Kumar, C. Ortix, M. Capone, and J. van den Brink, Phys. Rev. Lett. **109**, 107601 (2012).

[6] R. Nourafkan, G. Kotliar, and A.-M. S. Tremblay, Phys. Rev. B **90**, 220405 (2014).

[7] H. Sakai, J. Fujioka, T. Fukuda, D. Okuyama, D. Hashizume, F. Kagawa, H. Nakao, Y. Murakami, T. Arima, A. Q. R. Baron, Y. Taguchi, and Y. Tokura, Phys. Rev. Lett. **107**, 137601 (2011).

[8] V. Goian, F. Kadlec, C. Kadlec, B. Dabrowski, S. Kolesnik, O. Chmaissem, D. Nuzhnyy, M. Kempa, V. Bovtun, M. Savinov, J. Hejtmánek, J. Prokleška, and S. Kamba, J. Phys. Condens. Matter **28**, 175901 (2016).

[9] V. Goian, E. Langenberg, N. Marcano, V. Bovtun, L. Maurel, M. Kempa, T. Prokscha, J. Kroupa, P. A. Algarabel, J. A. Pardo, and S. Kamba, Phys. Rev. B **95**, 075126 (2017).

[10] E. Langenberg, R. Guzmán, L. Maurel, L. Martínez de Baños, L. Morellón, M. R. Ibarra, J. Herrero-Martín, J. Blasco, C. Magén, P. A. Algarabel, and J. A. Pardo, ACS Appl. Mater. Interfaces **7**, 23967 (2015).

[11] R. Bujakiewicz-Koronska, D. M. Nalecz, A. M. Majcher, E. Juszynska-Galazka, M. Galazka, L. Vasylechko, E. Markiewicz, D. Majda, A. Kalvane, and K. Koronski, J. Eur. Ceram. Soc. **37**, (2017).

[12] J. Hong, A. Stroppa, J. Íñiguez, S. Picozzi, and D. Vanderbilt, Phys. Rev. B **85**, 054417 (2012).

[13] D. K. Pratt, J. W. Lynn, J. Mais, O. Chmaissem, D. E. Brown, S. Kolesnik, and B.

Dabrowski, Phys. Rev. B **90**, 140401 (2014).

[14] E. Langenberg, L. Maurel, N. Marcano, R. Guzmán, P. Štrichovanec, T. Prokscha, C. Magén, P. A. Algarabel, and J. A. Pardo, Adv. Mater. Interfaces **4**, 1601040 (2017).

[15] B. Noheda, D. E. Cox, G. Shirane, J. A. Gonzalo, L. E. Cross, S.-E. Park, Appl. Phys. Lett. 74, 2059 (1999).

[16] L. Bellaiche, A. García, and D. Vanderbilt, Phys. Rev. Lett. **84**, 5427 (2000).

[17] M. Ahart, M. Somayazulu, R. E. Cohen, P. Ganesh, P. Dera, H.-K. Mao, R. J. Hemley, Y. Ren, P. Liermann, and Z. Wu, Nature **451**, 545 (2008).

[18] R. J. Zeches, M. D. Rossell, J. X. Zhang, A. J. Hatt, Q. He, C.-H. Yang, A. Kumar, C. H. Wang, A. Melville, C. Adamo, G. Sheng, Y.-H. Chu, J. F. Ihlefeld, R. Erni, C. Ederer, V. Gopalan, L. Q. Chen, D. G. Schlom, N. A. Spaldin, L. W. Martin, and R. Ramesh, Science **326**, 977 (2009).

[19] W. Jo, J. E. Daniels, J. L. Jones, X. Tan, P. A. Thomas, D. Damjanovic, and J. Rödel, J. Appl. Phys. **109**, 14110 (2011).

[20] L. Chen, Y. Yang, Z. Gui, D. Sando, M. Bibes, X. K. Meng, and L. Bellaiche, Phys. Rev. Lett. **115**, 267602 (2015).

[21] L. Zhang, M. Zhang, L. Wang, C. Zhou, Z. Zhang, Y. Yao, L. Zhang, D. Xue, X. Lou, and X. Ren, Appl. Phys. Lett. **105**, 162908 (2014).

[22] A. Prasatkhetragarn, N. Vittayakorn, S. Ananta, R. Yimnirun, and D. P. Cann, Jpn. J. Appl. Phys. **47**, 998 (2008).

[23] H. J. Zhao, W. Ren, Y. Yang, J. Íñiguez, X. M. Chen, and L. Bellaiche, Nat. Commun. **5**, 4021 (2014).

[24] E. O. Wollan and W. C. Koehler, Phys. Rev. **100**, 545 (1955).

[25] G. Kresse and J. Furthmüller, Phys. Rev. B **54**, 11169 (1996).

[26] P. Hohenberg and W. Kohn, Phys. Rev. **136**, B864 (1964).

[27] W. Kohn and L. J. Sham, Phys. Rev. **140**, A1133 (1965).

[28] J. P. Perdew, K. Burke, and M. Ernzerhof, Phys. Rev. Lett. **77**, 3865 (1996).

[29] A. I. Liechtenstein, V. I. Anisimov, and J. Zaanen, Phys. Rev. B **52**, R5467 (1995).

[30] G. Kresse and D. Joubert, Phys. Rev. B **59**, 1758 (1999).

[31] P. E. Blöchl, Phys. Rev. B **50**, 17953 (1994).

[32] R. D. King-Smith and D. Vanderbilt, Phys. Rev. B **47**, 1651 (1993).

[33] H. T. Stokes and D. M. Hatch, J. Appl. Cryst. J. Appl. Cryst **38**, 237 (2005).

[34] A. Ohtomo and H. Y. Hwang, Nature **427**, 423 (2004).

[35] T. Ichinose, H. Naganuma, K. Mukaiyama, M. Oogane, and Y. Ando, J. Cryst. Growth

409, 18 (2015).

[36] L. Bellaiche and D. Vanderbilt, Phys. Rev. Lett. **83**, 1347 (1999).

[37] L. Wollmann, S. Chadov, J. Kübler, and Claudia Felser, Phys. Rev. B 92, 064417 (2015).

[38] J. Winterlik *et al.*, Adv. Mater. 24, 6283 (2012).

[39] J.H. Lee and K.M. Rabe, Phys. Rev. Lett. **104**, 207204 (2010).

[40] Z. Chen, S. Prosandeev, Z. L. Luo, W. Ren, Y. Qi, C. W. Huang, L. You, C. Gao, I. A. Kornev, T. Wu, J. Wang, P. Yang, T. Sritharan, L. Bellaiche, and Lang Chen, Physical Review B 84, 094116 (2011).

[41] J. P. Perdew, A. Ruzsinszky, G. I. Csonka, O. A. Vydrov, G. E. Scuseria, L. A. Constantin, X. Zhou, and K. Burke, Phys. Rev. Lett. **100**, 136406 (2008)

Table 1

Hubbard U (eV)	P(C/m^2)	a_{ip} (Å)	c/a	magnetic moment (μ_B)
2	0.3517	3.8579	1.0322	2.469
3	0.2934	3.8690	1.0219	2.566
4.5	0.1764	3.8847	1.0076	2.708

Table Captions:

Table 1. Dependence of the Hubbard U parameter on the polarization, in-plane lattice constant, axial ratio and magnetic moment of Mn ions of the predicted equilibrium tetragonal state of G-AFM-arranged $Sr_{0.5}Ba_{0.5}MnO_3$ bulk, as mimicked by the DP structure and using the PBE+U+J functional with J=1.0 eV.

Table 2

	Hubbard U (eV)	ΔE (meV)	magnetic moment (μ_B)
A	2.0	66.58	2.559
	3.0	60.85	2.645
	4.5	55.72	2.805
C	2.0	58.46	2.468
	3.0	53.90	2.567
	4.5	54.34	2.733
FM	2.0	83.42	2.587
	3.0	73.76	2.674
	4.5	61.80	2.840

Table Captions:

Table 2. Magnetic moment of Mn ions and energy difference (ΔE) of A-AFM, C-AFM and FM arrangements with respect to the G-AFM configuration of $Sr_{0.5}Ba_{0.5}MnO_3$ bulk (as mimicked by the DP structure) for different Hubbard U parameters, using the PBE+U+J functional with J=1.0 eV.

Figure Captions

Figure 1. (Left) Rock-salt ordered structure (DP) and (Right) layered chemical arrangement (DL) presently used to investigate $Sr_{0.5}Ba_{0.5}MnO_3$. Note the a-axis shown here lies along the pseudo-

cubic [-1-10] direction, while the b-axis is along [1-10]. The c-axis is parallel to the out-of-plane [001] direction.

Figure 2. Properties of the SBM films, as mimicked by the DP structure and using PBE+U+J functionals with U= 3eV and J=1 eV, as a function of their in-plane lattice parameter. Panel (a) shows the total energy of the I4mm, Cm and Imm2 states, for the four studied magnetic arrangements. The arrows show the local maxima of the monoclinic structure for the G-AFM and FM orderings. Panel (b) displays the out-of-plane and in-plane components of the polarization in the different magnetic ground states, while Panel (c) reports the associated evolution of the axial ratio. The vertical dashed lines denote the magnetic transitions in Panels (b) and (c).

Figure 3. Lowest optical frequency at the Γ-point for the G-type AFM configuration as a function of the in-plane lattice parameter in the DP structure, when using the PBE+U+J functional with U= 3.0 eV and J=1.0 eV.

Figure 4. Influence of Hubbard U on the total energy of the SBM films for the DP structure using PBE+U+J functionals with U=2.0eV; 3.0eV; 4.5eV and J=1.0 eV as a function of the in-plane lattice constant.

Figure 5. Properties of the SBM films, as mimicked by the DL structure and using PBE+U+J functionals with U= 3eV and J=1 eV, as a function of their in-plane lattice parameter. Panel (a) shows the total energy of the P4mm, Cm and Amm2 states, for the four studied magnetic arrangements. The arrows show the local maxima of the monoclinic structure for the G-AFM and FM orderings. Panel (b) displays the out-of-plane and in-plane components of the polarization in the different magnetic ground states, while Panel (c) reports the associated evolution of the axial ratio. The vertical dashed lines denote the magnetic transitions in Panels (b) and (c).

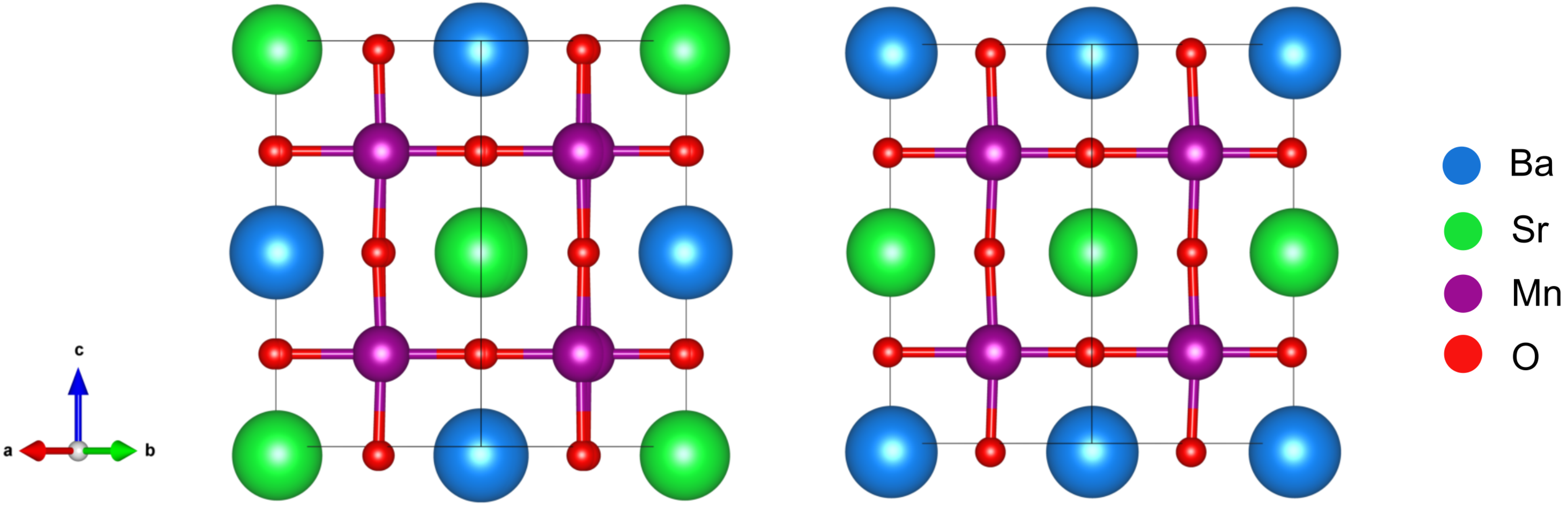
c
a
b
Ba
Sr
Mn
O

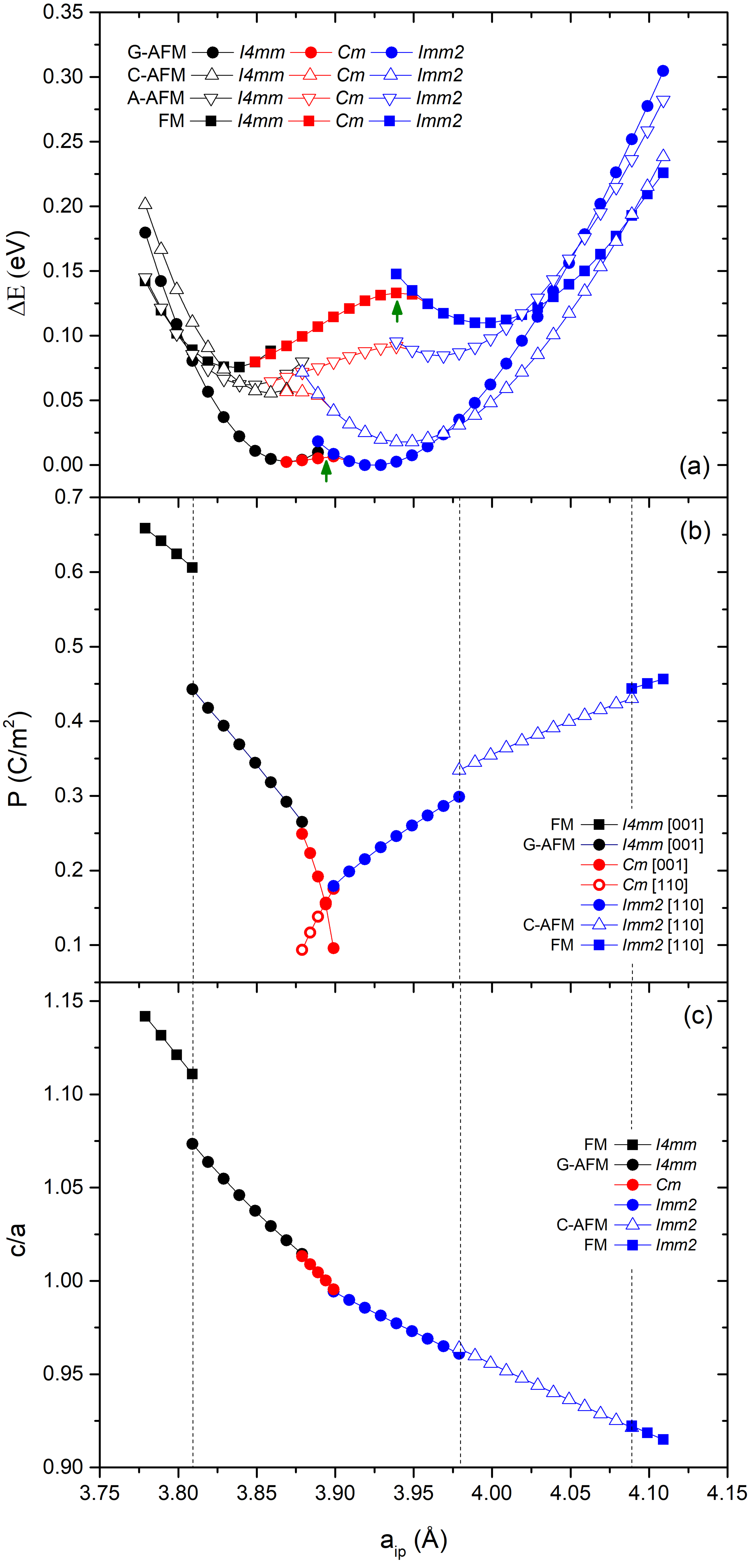
G-AFM I4mm Cm Imm2
C-AFM I4mm Cm Imm2
A-AFM I4mm Cm Imm2
FM I4mm Cm Imm2
(a)
ΔE (eV)
0.35
0.30
0.25
0.20
0.15
0.10
0.05
0.00
(b)
P (C/m^2)
0.7
0.6
0.5
0.4
0.3
0.2
0.1
FM I4mm [001]
G-AFM I4mm [001]
Cm [001]
Cm [110]
Imm2 [110]
C-AFM Imm2 [110]
FM Imm2 [110]
(c)
c/a
1.15
1.10
1.05
1.00
0.95
0.90
FM I4mm
G-AFM I4mm
Cm
Imm2
C-AFM Imm2
FM Imm2
3.75
3.80
3.85
3.90
3.95
4.00
4.05
4.10
4.15
a$_{ip}$ (Å)

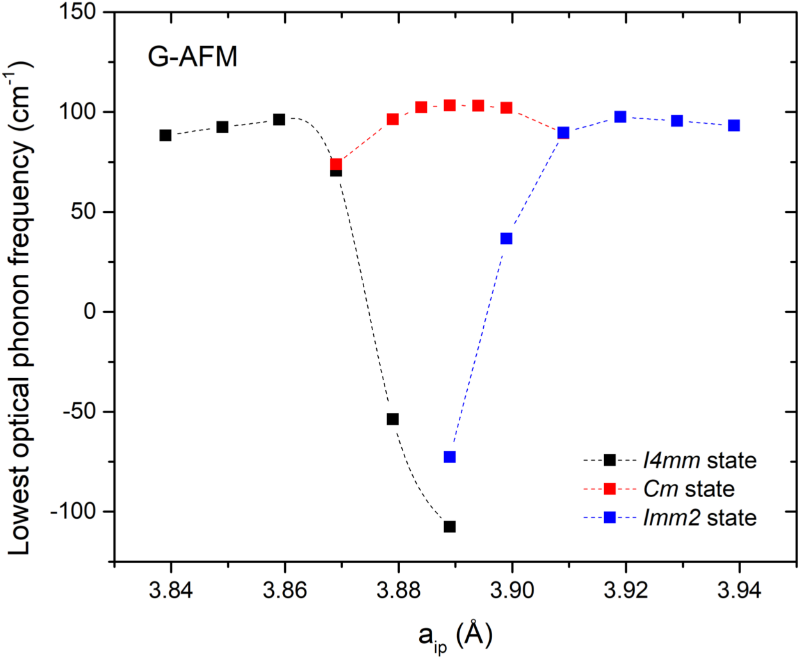
G-AFM
Lowest optical phonon frequency (cm^{-1})
150
100
50
0
-50
-100
3.84
3.86
3.88
3.90
3.92
3.94
a$_{ip}$ (Å)
I4mm state
Cm state
Imm2 state

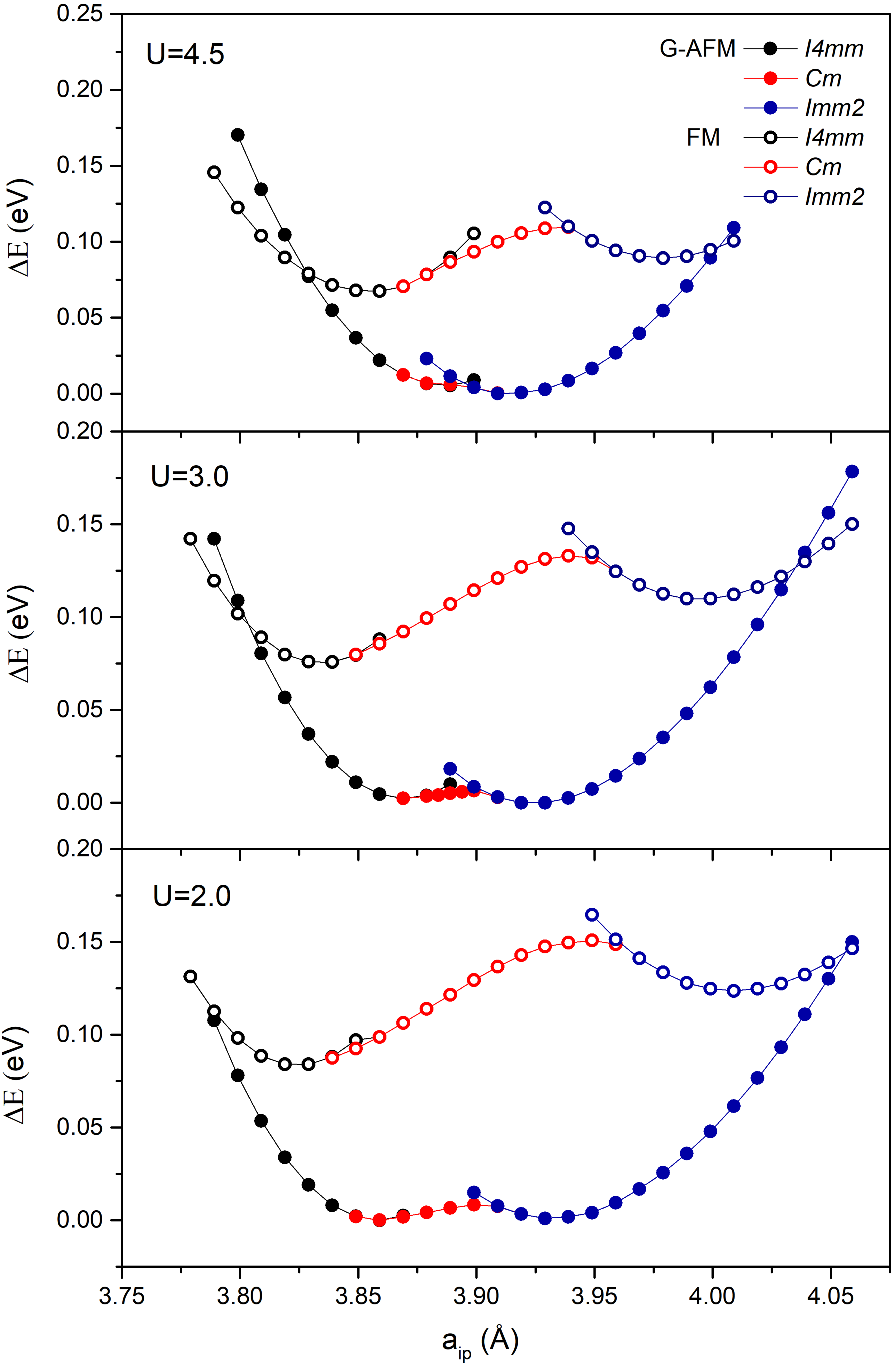
U=4.5
G-AFM
I4mm
Cm
Imm2
FM
I4mm
Cm
Imm2
U=3.0
U=2.0
ΔE (eV)
0.25
0.20
0.15
0.10
0.05
0.00
3.75
3.80
3.85
3.90
3.95
4.00
4.05
a_ip (Å)

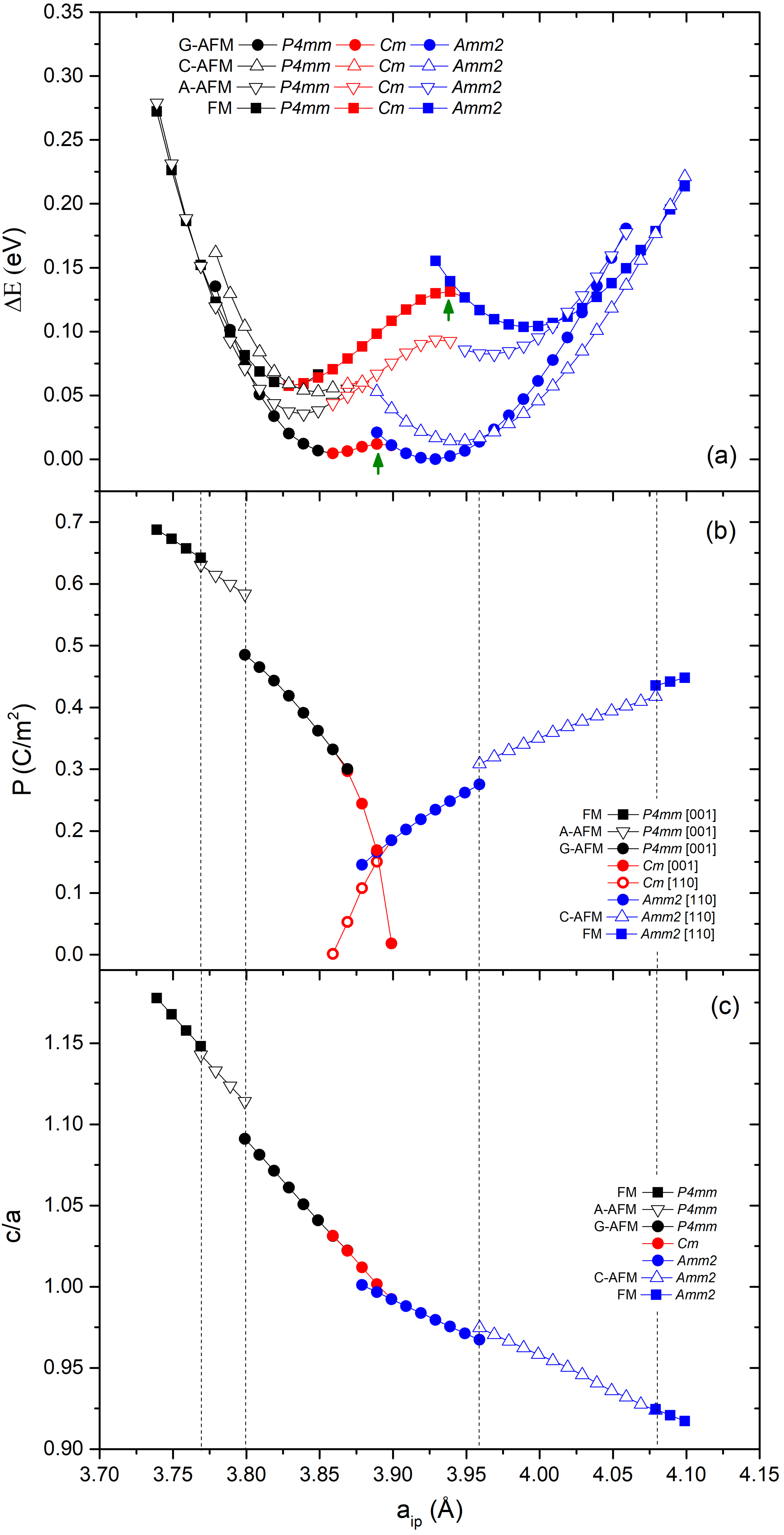
G-AFM P4mm Cm Amm2
C-AFM P4mm Cm Amm2
A-AFM P4mm Cm Amm2
FM P4mm Cm Amm2
ΔE (eV)
0.35
0.30
0.25
0.20
0.15
0.10
0.05
0.00
(a)
P (C/m^2)
0.7
0.6
0.5
0.4
0.3
0.2
0.1
0.0
(b)
FM P4mm [001]
A-AFM P4mm [001]
G-AFM P4mm [001]
Cm [001]
Cm [110]
Amm2 [110]
C-AFM Amm2 [110]
FM Amm2 [110]
c/a
1.15
1.10
1.05
1.00
0.95
0.90
(c)
FM P4mm
A-AFM P4mm
G-AFM P4mm
Cm
Amm2
C-AFM Amm2
FM Amm2
3.70
3.75
3.80
3.85
3.90
3.95
4.00
4.05
4.10
4.15
a$_{ip}$ (Å)